AIMS Mathematics, 11(3): 6910–6934.
DOI: 10.3934/math.2026284
Received: 19 December 2025
Revised: 05 March 2026
Accepted: 10 March 2026
Published: 17 March 2026

https://www.aimspress.com/journal/Math

Research article

Trilinearization of the Kairat-II equation for the soliton solutions with machine learning evolution and Painlevé analysis

Waseem Razzaq[1], **Asim Zafar**[1], **Naif Almusallam**[2,*] **and Fawaz Khaled Alarfaj**[2]

[1] Department of Mathematics, COMSATS University Islamabad, Vehari Campus, Pakistan
[2] Department of Management Information Systems, School of Business, King Faisal University, Al-Ahsa 31982, Saudi Arabia

* **Correspondence:** Email: nalmuslem@kfu.edu.sa.

Abstract: This research examines the integrability and soliton solution in different forms of the Kairat-II equation. A thorough Painlevé analysis determines that the equation fulfills the criteria of compatibility conditions for integrability; thus, it is shown to exhibit soliton solutions. Applying the Hirota D-operator, we transform the Kairat-II equation into a trilinear form. This enables the derivation of precise analytical solutions, including novel breather wave and three-wave soliton solutions by the Hirota method. These solutions reveal localized, oscillatory, and energy-exchange structures, capturing the complex nonlinear dynamics of the model. We use a machine learning analysis, the multi-layer perceptron regressor algorithm, for understanding the dynamics of these solitons, which effectively predicts the progression and dynamics of the obtained solutions. The analytical results are validated and displayed in 2D and 3D+contour plots using symbolic computation tools such as Mathematica and Python. In the end, we execute the asymptotic analysis on the gained solution and present the asymptotic behavior of the solutions. We can learn a great deal about the intricate dynamics that the Kairat-II model governs from these visualizations.

Keywords: Kairat-II equation; Painlevé analysis; trilinear form; Hirota method; three-wave and Breather-wave solutions; machine learning; asymptotic analysis
Mathematics Subject Classification: 35A20, 35C08, 35Q55, 37K10

1. Introduction

Nonlinear partial differential equations (NPDEs) play a crucial role in various areas of applied sciences, including chemistry, biology, optics, economics, electromagnetism, fluid dynamics, solid mechanics, elasticity, engineering quantum mechanics, and more. Many naturally occurring phenomena can be modeled by NPDEs; for example, the Newell-Whitehead-Segel equation [1], the

Harry Dym equation [2], the Schrödinger equation [3], the Telegraph and Kolmogorov-Petrovskii-Piskunov equations [4], the Westervelt model [5], the biological population equation [6], the diffusion-reaction equation [7], the Schrödinger–Korteweg–de Vries (KdV) equations [8], the Jaulent-Miodek equations and coupled Konno-Oono systems [9], the Fokas system [10], the sinh-Gordon equation [11], the stochastic potential Yu–Toda–Sasa–Fukuyama equation [12], the perturbed modified Gardner equation [13], the (3+1)-dimensional extended Kairat-X equation [14], and the 2D Allen-Cahn equation [15]. In this research, our discussion is about the Kairat-II equation. In [16], authors investigated the Karait-II equation from the Kairat-I equation by putting some suitable values in Kairat-I, and investigators found the NPD Kairat-II equation and traveling wave solutions. Before this, the Kairat-II equation had been solved by the Paul-Painlevé approach to construct the Lie point symmetry in [17], by the extended algebraic method to develop the solitary solutions in [18], and by the generalized Kudryashov, the epx_a function, and modified simplest equation methods in [19]. The solitary wave solutions were obtained from the (3+1)-dimensional Kairat-II by the two analytical techniques, like modified extended tanh expansion and the modified generalized Raccati equation mapping method [20], and lump and breather wave solutions were obtained by the Hirota bilinear method in [21]. Numerous different strategies were put into execution to gain the distinct forms of exact solitons i.e, the Hirota bilinear technique [22], the modified extended tanh expansion scheme [23], the solitary wave ansatz scheme [24], the $\exp(-\phi(\xi))$-expansion technique [25], the (G'/G)-expansion method [26], the $\exp_a$ function scheme [27], the extended Sinh–Gordon equation expansion scheme [28], and more. In this study, we execute the Hirota method with trilinear form [29]. In that work, authors studied different types of results, like breather wave, lump wave, breather-kink wave, and lump-kink wave. In [30], investigators gained the Wronskian n-soliton solutions of the generalized KdV equation of trilinear form; in [31], researchers found the multi-soliton solutions of the extended second Kadomtsev–Petviashvili equation in trilinear form; in [32], the investigators obtained multi-solitons, M-lumps and fusion solitons of the Bogoyavlenskii–Schieff equation in trilinear form; and in [33], researchers acquired the dark and bright rogue wave and lump type solutions of the Nizhnik–Novikov–Veselov equation in trilinear form.

In this research, we execute the Painlevé analysis on the Kairat-II equation in order to determine its integrability. The Painlevé analysis is a widely used tool for identifying the integrability of nonlinear models. This idea has been successfully applied to a variety of equations by numerous scholars. In [34], the authors validated the integrability of the Painlevé analysis by applying it to the generalized Burgers system. The Painlevé analysis was used on the extended Sakovich equation in [35], and the researchers showed that it complied with the integrability requirements. Similarly, the authors of [36] investigated and verified the integrability of a generalized (3 + 1)-dimensional Painlevé-type nonlinear evolution equation.

We employ machine learning in our study to enhance performance and facilitate better predictions. System learning enables a system to analyze data and generate predictions autonomously, without explicit instructions. Machine learning encompasses various types, as well as supervised learning, unsupervised learning, and reinforcement learning. This study is motivated by supervised learning, where the available dataset is divided into training and testing sets in order to predict outputs from given inputs. Specifically, we employ the multilayer perceptron (MLP) regressor algorithm based on a neural network [37] to expect wave dynamics from the actual data. The present study is undertaken with the following key objectives:

- To validate the integrability of the model through Painlevé analysis.
- To derive novel analytical solutions to the Kairat-II equation, including soliton, breather wave, and three-wave solutions, using the Hirota method with trilinear form.
- To apply a machine learning algorithm for predicting the wave dynamics of the obtained solutions.
- To visualize all findings through comprehensive 2D and 3D+contour plots, accompanied by interpreted parameters and physically descriptive captions.
- To execute asymptotic analysis on the gain solutions to check their asymptotic behavior.

Figure 1 shows the study of the article.

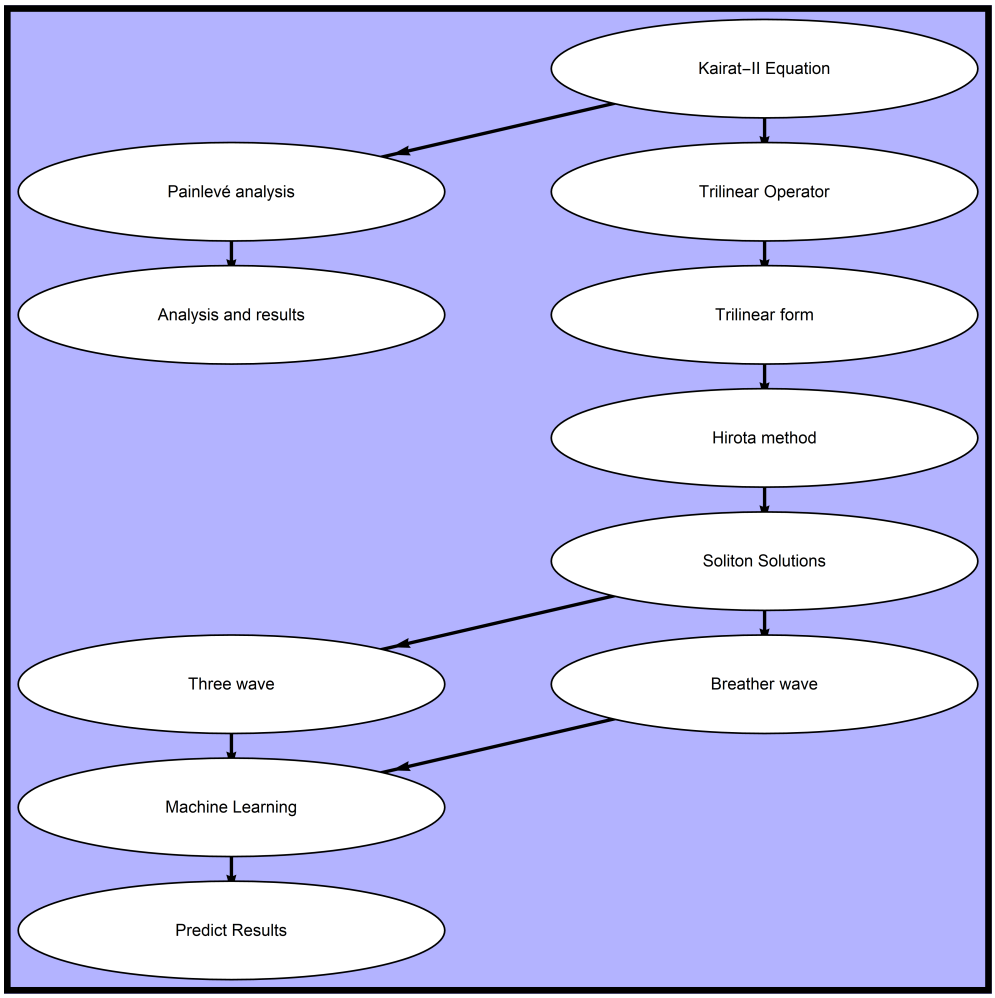

Figure 1. Flowchart of study in the article.

The article is prepared as follows: Section 2 presents the model description and its applications. Section 3 presents the Painlevé analysis and its results. Section 4 outlines the trilinear form and the model under consideration. Section 5 discusses the derived soliton solutions. Section 6 provides graphical representations of the results. Section 7 describes the machine learning methodology employed. Section 8 presents the results and their discussion. Section 9 presents asymptotic analysis. Section 10 concludes the study.

2. Model and its applications

The Kairat-II equation is an NPDE that describes complex wave propagation phenomena in certain physical systems. This equation can be written as

$$u_{xt} - 2u_{xx}u_t - 4u_{xt}u_x + u_{xxxt} = 0. \tag{2.1}$$

2.1. Applications

The Kairat-II equation arises in various physical contexts, including:

- **Nonlinear wave propagation:** It models the evolution of wave packets in shallow water or plasma where higher-order nonlinear interactions are significant.
- **Optical fibers:** It describes the dynamics of ultrashort pulse propagation in nonlinear optical media.
- **Fluid mechanics:** The equation can represent the interaction of long waves in a dispersive medium with nonlinear effects.

3. Description of Painlevé analysis

Consider an NPDE of the form

$$H(v, v_{\sigma_1}, v_{\sigma_2}, v_{\sigma_1\sigma_2}, v_{\sigma_1\sigma_1}, v_{\sigma_2\sigma_2}, ...) = 0. \tag{3.1}$$

The associated singular manifold is described by

$$F(\sigma_1, \sigma_2, ..., \sigma_n) = 0. \tag{3.2}$$

A Laurent series expansion is assumed as the solution of Eq (3.1):

$$v(\sigma_1, \sigma_2, ..., \sigma_n) = F^{\mu}(\sigma_1, \sigma_2, ..., \sigma_n) \sum_{i=0}^{\infty} v_i(\sigma_1, \sigma_2, ..., \sigma_n) F^i(\sigma_1, \sigma_2, ..., \sigma_n). \tag{3.3}$$

Here, v and v_i are arbitrary functions of $(\sigma_1, \sigma_2, \ldots, \sigma_n)$, and μ is a non-positive integer. The Painlevé analysis proceeds as follows:

Step 1: Determine the value of μ by substituting

$$v = F^{\mu} v_0 \tag{3.4}$$

in Eq (3.1).

Step 2: Get the value of v_0 from the coefficient of the leading order term.

Step 3: Substitute

$$v = F^{\mu} v_0 + \sum_{i=1}^{\infty} v_i F^{i+\mu} \tag{3.5}$$

in Eq (3.1) to determine the resonance values of i.

Step 4: Extend the series (3.3) up to the largest resonance value $i = r_{\max}$:

$$v = \sum_{i=0}^{r_{max}} v_i F^{i+\mu}. \tag{3.6}$$

The functions v_i are then determined sequentially.

Step 5: The compatibility condition for the Painlevé property requires that the coefficients v_i corresponding to resonance values appear as arbitrary functions. If this criterion is satisfied for the obtained resonance values, Eq (3.1) possesses the Painlevé property and is thus Painlevé integrable.

3.1. Inegrability of the Kairat-II equation

In this part, we perform the Painlevé analysis for the nonlinear Kairat-II equation. The associated singular manifold is given by

$$F(x,t) \ = 0. \tag{3.7}$$

The result of Eq (2.1) is assumed in the form of Eq (3.5), where v, v_i, and F are functions of x and t. To determine the values of μ and v_0, we substitute Eq (3.4) into Eq (2.1), yielding

$$\mu = -1, \quad v_0 = -2F_x. \tag{3.8}$$

Next, the resonance values are obtained by inserting Eq (3.6) in Eq (2.1), we derive

$$i = -1,\ 1,\ 4,\ 6.$$

The largest resonance value is $r_{\max} = 6$, and hence the Laurent series (3.6) can be extended as:

$$v = F^{-1}v_0 + v_1 + v_2F + v_3F^2 + v_4F^3 + v_5F^4 + v_6F^5. \tag{3.9}$$

Substituting Eq (3.9) into Eq (2.1) yields the following coefficients:

$$v_2 = \frac{F_t\left(2F_xF_{\rm xxx} + F_x^2 - F_{\rm xx}^2\right) + 2F_x\left(F_xF_{\rm xxt} - F_{\rm xt}F_{\rm xx}\right)}{6F_tF_x^3}, \tag{3.10}$$

$$v_3 = \frac{1}{12F_t^2F_x^5}(2F_tF_x(F_{xt}(2F_xF_{xxx} - 3F_{xx}^2) + F_x(3F_{xx}F_{xxt} - 2F_xF_{xxxt})) \tag{3.11}$$

$$+ F_t^2(4F_xF_{xx}F_{xxx} + F_x^2(F_{xx} - F_{xxxx}) - 2F_{xx}^3) + 4F_x^2F_{xt}(F_xF_{xxt} - F_{xt}F_{xx})), \tag{3.12}$$

$$v_5 = \frac{1}{108F_t^5F_x^5}(35F_{\rm xx}^5 - 62F_xF_{\rm xxx}F_{\rm xx}^3... + 45F_{\rm tt}F_xF_{\rm xt}^2(F_{xt}F_{xx} - F_xF_{xxt})). \tag{3.13}$$

The obtained resonances at $i = -1, 1, 4, 6$ indicate that v_1, v_4, and v_6 are arbitrary functions associated with the singular manifold. Therefore, the compatibility criteria of the Painlevé analysis are satisfied, and Eq (2.1) possesses the Painlevé property, implying that the Kairat-II equation is integrable.

4. The trilinearization of the problem

The Hirota formula is

$$\prod_{i=1}^{j} \mathrm{D}_{y_i}^{n_i}\Omega.\,\Delta = \prod_{i=1}^{j}\left(\frac{\partial}{\partial y_i} - \frac{\partial}{\partial y_i'}\right)^{n_i} \Omega(y_1,...,y_j)\Delta(y_1',...,y_j')\Big|_{y_1=y_1',...,y_j=y_j'},$$

and the trilinear operators [29], are defined as

$$\begin{aligned}&\prod_{i=1}^{j} \mathrm{D}_{y_i}^{n_i}\,\Omega\cdot\Delta\cdot f\\ &=\prod_{i=1}^{j}\left(\Lambda_{pi}\frac{\partial}{\partial y_i} + \Lambda_{pi}'\frac{\partial}{\partial y_i'} + \Lambda_{pi}''\frac{\partial}{\partial y_i''}\right)^{n_i} \Omega(y_1,...,y_j)\Delta(y_1',...,y_j'), f(y_1'',...,y_j'')\Big|_{y_1=y_1'=y_1'',...,y_j=y_j'=y_j''},\end{aligned}$$

where the powers of

$$\Lambda_m = (-1)^{Q_m^n}, \quad (m \geq 1),$$

with $n \equiv Q_m^n \mod m$, $0 \leq Q_m^n \leq m$, and $n \geq 0$. The powers Q_m^n have the following signs:

$$\begin{aligned} m = 2k\ (k \in \mathbb{N}): &\quad 1,-1,1,-1,\ldots,\\ m = 1: &\quad 1,1,1,1,\ldots,\\ m = 3: &\quad 1,-1,1,-1,\ldots,\\ m = 5: &\quad 1,-1,1,-1,1,-1,\ldots,\\ &\vdots\end{aligned}$$

Now for $n = 0, 1, 2, \ldots$, if we take $y_i = \langle y_i, y_i', y_i''\rangle = \langle 1, 2, 3\rangle$ and $\Omega = \lambda = f$, it becomes

$$\begin{aligned}&\mathrm{D}_x^2 f\cdot f\cdot f = 3f_{xx}f^2 - 2f_x^2 f,\\ &\mathrm{D}_t^2 f\cdot f\cdot f = 3f_{tt}f^2 - 2f_y^2 f,\\ &\mathrm{D}_x\mathrm{D}_t f\cdot f\cdot f = 3f_{xt}f^2 - 2f_x f_t f,\\ &\mathrm{D}_x^4 f\cdot f\cdot f = f_{xxxx}f^2 - 8f_{xxx}f_x f - 12f_{xx}^2 f + 18f_x^2 f_{xx},\\ &\mathrm{D}_x^3\mathrm{D}_t f\cdot f\cdot f = f_{xxxt}f^2 - 2f_{xxx}f_t f - 6f_{xxt}f_x f - 6f_{xx}f_{xt}f - 6f_{xt}f_x^2 + 18f_x f_{xx}f_t,\\ &\qquad\vdots\end{aligned}$$

Applying the transformation $u = -2(\ln f)_x$, Eq (2.1) can be reformulated into the following trilinear form:

$$\begin{aligned}&-2f^2 f_{\mathrm{xxt}} - 2f^2 f_{\mathrm{xxxxt}} - 8f_t f_x f_{\mathrm{xxx}} - 4f_t f_x^2 + 2ff_t f_{\mathrm{xx}} + 4f_t f_{\mathrm{xx}}^2\\ &+2ff_t f_{\mathrm{xxxx}} + 8f_x f_{\mathrm{xt}} f_{\mathrm{xx}} + 4ff_x f_{\mathrm{xt}} - 8f_x^2 f_{\mathrm{xxt}} + 8ff_x f_{\mathrm{xxxt}} - 4ff_{\mathrm{xx}} f_{\mathrm{xxt}} = 0.\end{aligned} \tag{4.1}$$

In terms of the D-operators, it can be expressed as

$$(\mathrm{D}_x^2\mathrm{D}_t - \mathrm{D}_x^4\mathrm{D}_t)f.f.f = 0. \tag{4.2}$$

5. Analytical soliton solutions

5.1. Breather-wave solution

Consider the transformation to attain the breather-wave outcomes [22]:

$$\begin{cases} \varsigma_1 = c_1 t + x, \\ \varsigma_2 = c_2 t + x, \\ f(\zeta) = \mathrm{e}^{-p_1\varsigma_1} + \kappa_1 \cos(p\varsigma_2) + \kappa_2 \mathrm{e}^{p_1\varsigma_1}. \end{cases} \tag{5.1}$$

By putting Eq (5.1) into Eq (4.1), done co-efficient of every order of including functions and their products. By setting these expressions equal to zero and solving the resulting algebraic system, we obtain multiple solution sets, which are presented as follows:

Set 1:

$$\{p_1 = -\frac{\mathrm{i}}{2},\ c_1 = c_1,\ c_2 = c_2,\ \kappa_1 = 0,\ \kappa_2 = \kappa_2,\ p = p\}, \tag{5.2}$$

$$u(x,t) = -\frac{\mathrm{i}\left(1 - \kappa_2 \mathrm{e}^{\mathrm{i}(c_1 t + x)}\right)}{1 + \kappa_2 \mathrm{e}^{\mathrm{i}(c_1 t + x)}}. \tag{5.3}$$

Set 2:

$$\{p_1 = \frac{\mathrm{i}}{2},\ c_1 = c_1,\ c_2 = c_2,\ \kappa_1 = 0,\ \kappa_2 = \kappa_2,\ p = p\}, \tag{5.4}$$

$$u(x,t) = -\frac{\mathrm{i}\left(-1 + \kappa_2 \mathrm{e}^{i(c_1 t + x)}\right)}{1 + \kappa_2 \mathrm{e}^{\mathrm{i}(c_1 t + x)}}. \tag{5.5}$$

Set 3:

$$\{c_1 = -c_2,\ p_1 = -\mathrm{i}p,\ \kappa_1 = -2\sqrt{\kappa_2}\}, \tag{5.6}$$

$$u(x,t) = -\frac{2\left(-\mathrm{i}\kappa_2 p \mathrm{e}^{-\mathrm{i}p(x-c_2 t)} + 2\sqrt{\kappa_2} p \sin\left(p\left(c_2 t + x\right)\right) + \mathrm{i}p\mathrm{e}^{\mathrm{i}p(x-c_2 t)}\right)}{\kappa_2 \mathrm{e}^{-\mathrm{i}p(x-c_2 t)} - 2\sqrt{\kappa_2}\cos\left(p\left(c_2 t + x\right)\right) + \mathrm{e}^{\mathrm{i}p(x-c_2 t)}}. \tag{5.7}$$

Set 4:

$$\{c_1 = -c_2,\ p_1 = -\mathrm{i}p,\ \kappa_1 = 2\sqrt{\kappa_2}\}, \tag{5.8}$$

$$u(x,t) = -\frac{2\left(-\mathrm{i}\kappa_2 p \mathrm{e}^{-\mathrm{i}p(x-c_2 t)} - 2\sqrt{\kappa_2} p \sin\left(p\left(c_2 t + x\right)\right) + \mathrm{i}p\mathrm{e}^{\mathrm{i}p(x-c_2 t)}\right)}{\kappa_2 \mathrm{e}^{-\mathrm{i}p(x-c_2 t)} + 2\sqrt{\kappa_2}\cos\left(p\left(c_2 t + x\right)\right) + \mathrm{e}^{\mathrm{i}p(x-c_2 t)}}. \tag{5.9}$$

Set 5:

$$\{c_1 = -c_2,\ p_1 = \mathrm{i}p,\ \kappa_1 = -2\sqrt{\kappa_2}\}, \tag{5.10}$$

$$u(x,t) = -2\left(\frac{\mathrm{i}\kappa_2 p \mathrm{e}^{\mathrm{i}p(x-c_2 t)} + 2\sqrt{\kappa_2} p \sin\left(p\left(c_2 t + x\right)\right) + (-\mathrm{i})p\mathrm{e}^{-\mathrm{i}p(x-c_2 t)}}{\kappa_2 \mathrm{e}^{\mathrm{i}p(x-c_2 t)} - 2\sqrt{\kappa_2}\cos\left(p\left(c_2 t + x\right)\right) + \mathrm{e}^{-\mathrm{i}p(x-c_2 t)}}\right). \tag{5.11}$$

Set 6:

$$\{c_1 = -c_2,\ p_1 = \mathrm{i}p,\ \kappa_1 = 2\sqrt{\kappa_2}\}, \tag{5.12}$$

$$u(x,t) = -\frac{2\left(\mathrm{i}\kappa_2 p \mathrm{e}^{\mathrm{i}p(x-c_2 t)} - 2\sqrt{\kappa_2} p \sin\left(p\left(c_2 t + x\right)\right) + (-\mathrm{i})p\mathrm{e}^{-\mathrm{i}p(x-c_2 t)}\right)}{\kappa_2 \mathrm{e}^{\mathrm{i}p(x-c_2 t)} + 2\sqrt{\kappa_2}\cos\left(p\left(c_2 t + x\right)\right) + \mathrm{e}^{-\mathrm{i}p(x-c_2 t)}}. \tag{5.13}$$

Set 7:

$$\{c_1 = -\frac{c_2 p}{p+1},\ p_1 = -\sqrt{-(p+1)^2},\ \kappa_1 = -\frac{2\sqrt{\kappa_2}(p+1)}{p}\}, \tag{5.14}$$

$$u(x,t) = -2\left(\frac{-\kappa_2\sqrt{-(p+1)^2}\mathrm{e}^{\sqrt{-(p+1)^2}\left(\frac{c_2 pt}{p+1}-x\right)} + 2\sqrt{\kappa_2}(p+1)\sin(p(c_2t+x)) + \sqrt{-(p+1)^2}\mathrm{e}^{\sqrt{-(p+1)^2}\left(x-\frac{c_2 pt}{p+1}\right)}}{\kappa_2\mathrm{e}^{\sqrt{-(p+1)^2}\left(\frac{c_2 pt}{p+1}-x\right)} - \frac{2\sqrt{\kappa_2}(p+1)\cos(p(c_2t+x))}{p} + \mathrm{e}^{\sqrt{-(p+1)^2}\left(x-\frac{c_2 pt}{p+1}\right)}}\right). \tag{5.15}$$

Set 8:

$$\{c_1 = -\frac{c_2 p}{p+1},\ p_1 = -\sqrt{-(p+1)^2},\ \kappa_1 = \frac{2\sqrt{\kappa_2}(p+1)}{p}\}, \tag{5.16}$$

$$u(x,t) = -\frac{2\left(-\kappa_2\sqrt{-(p+1)^2}\mathrm{e}^{\sqrt{-(p+1)^2}\left(\frac{c_2 pt}{p+1}-x\right)} - 2\sqrt{\kappa_2}(p+1)\sin(p(c_2t+x)) + \sqrt{-(p+1)^2}\mathrm{e}^{\sqrt{-(p+1)^2}\left(x-\frac{c_2 pt}{p+1}\right)}\right)}{\kappa_2\mathrm{e}^{\sqrt{-(p+1)^2}\left(\frac{c_2 pt}{p+1}-x\right)} + \frac{2\sqrt{\kappa_2}(p+1)\cos(p(c_2t+x))}{p} + \mathrm{e}^{\sqrt{-(p+1)^2}\left(x-\frac{c_2 pt}{p+1}\right)}}. \tag{5.17}$$

Set 9:

$$\{c_1 = -\frac{c_2 p}{p+1},\ p_1 = \sqrt{-(p+1)^2},\ \kappa_1 = -\frac{2\sqrt{\kappa_2}(p+1)}{p}\}, \tag{5.18}$$

$$u(x,t) = -\frac{2\left(\kappa_2\sqrt{-(p+1)^2}\mathrm{e}^{\sqrt{-(p+1)^2}\left(x-\frac{c_2 pt}{p+1}\right)} + 2\sqrt{\kappa_2}(p+1)\sin(p(c_2t+x)) + \sqrt{-(p+1)^2}\left(-\mathrm{e}^{\sqrt{-(p+1)^2}\left(\frac{c_2 pt}{p+1}-x\right)}\right)\right)}{\kappa_2\mathrm{e}^{\sqrt{-(p+1)^2}\left(x-\frac{c_2 pt}{p+1}\right)} - \frac{2\sqrt{\kappa_2}(p+1)\cos(p(c_2t+x))}{p} + \mathrm{e}^{\sqrt{-(p+1)^2}\left(\frac{c_2 pt}{p+1}-x\right)}}. \tag{5.19}$$

Set 10:

$$\{c_1 = -\frac{c_2 p}{p+1},\ p_1 = \sqrt{-(p+1)^2},\ \kappa_1 = \frac{2\sqrt{\kappa_2}(p+1)}{p}\}, \tag{5.20}$$

$$u(x,t) = -\frac{2\left(\kappa_2\sqrt{-(p+1)^2}\mathrm{e}^{\sqrt{-(p+1)^2}\left(x-\frac{c_2 pt}{p+1}\right)} - 2\sqrt{\kappa_2}(p+1)\sin(p(c_2t+x)) + \sqrt{-(p+1)^2}\left(-\mathrm{e}^{\sqrt{-(p+1)^2}\left(\frac{c_2 pt}{p+1}-x\right)}\right)\right)}{\kappa_2\mathrm{e}^{\sqrt{-(p+1)^2}\left(x-\frac{c_2 pt}{p+1}\right)} + \frac{2\sqrt{\kappa_2}(p+1)\cos(p(c_2t+x))}{p} + \mathrm{e}^{\sqrt{-(p+1)^2}\left(\frac{c_2 pt}{p+1}-x\right)}}. \tag{5.21}$$

Set 11:

$$\{c_1 = -\frac{c_2 p}{p-1},\ p_1 = -\sqrt{-(p-1)^2},\ \kappa_1 = -\frac{2\sqrt{\kappa_2}(p-1)}{p}\}, \tag{5.22}$$

$$u(x,t) = -\frac{2\left(\kappa_2\sqrt{-(p-1)^2}\mathrm{e}^{\sqrt{-(p-1)^2}\left(x-\frac{c_2 pt}{p-1}\right)} + 2\sqrt{\kappa_2}(p-1)\sin(p(c_2t+x)) + \sqrt{-(p-1)^2}\left(-\mathrm{e}^{\sqrt{-(p-1)^2}\left(\frac{c_2 pt}{p-1}-x\right)}\right)\right)}{\kappa_2\mathrm{e}^{\sqrt{-(p-1)^2}\left(x-\frac{c_2 pt}{p-1}\right)} - \frac{2\sqrt{\kappa_2}(p-1)\cos(p(c_2t+x))}{p} + \mathrm{e}^{\sqrt{-(p-1)^2}\left(\frac{c_2 pt}{p-1}-x\right)}}. \tag{5.23}$$

Set 12:

$$\{c_1 = -\frac{c_2 p}{p-1},\ p_1 = -\sqrt{-(p-1)^2},\ \kappa_1 = \frac{2\sqrt{\kappa_2}(p-1)}{p}\}, \tag{5.24}$$

$$u(x,t) = -\frac{2\left(-\kappa_2\sqrt{-(p-1)^2}\mathrm{e}^{\sqrt{-(p-1)^2}\left(\frac{c_2 pt}{p-1}-x\right)} - 2\sqrt{\kappa_2}(p-1)\sin(p(c_2t+x)) + \sqrt{-(p-1)^2}\mathrm{e}^{\sqrt{-(p-1)^2}\left(x-\frac{c_2 pt}{p-1}\right)}\right)}{\kappa_2\mathrm{e}^{\sqrt{-(p-1)^2}\left(\frac{c_2 pt}{p-1}-x\right)} + \frac{2\sqrt{\kappa_2}(p-1)\cos(p(c_2t+x))}{p} + \mathrm{e}^{\sqrt{-(p-1)^2}\left(x-\frac{c_2 pt}{p-1}\right)}}. \tag{5.25}$$

Set 13:

$$\{c_1 = -\frac{c_2 p}{p-1},\ p_1 = \sqrt{-(p-1)^2},\ \kappa_1 = -\frac{2\sqrt{\kappa_2}(p-1)}{p}\}, \tag{5.26}$$

$$u(x,t) = -\frac{2\left(\kappa_2\sqrt{-(p-1)^2}\mathrm{e}^{\sqrt{-(p-1)^2}\left(x-\frac{c_2 pt}{p-1}\right)} + 2\sqrt{\kappa_2}(p-1)\sin(p(c_2t+x)) + \sqrt{-(p-1)^2}\left(-\mathrm{e}^{\sqrt{-(p-1)^2}\left(\frac{c_2 pt}{p-1}-x\right)}\right)\right)}{\kappa_2\mathrm{e}^{\sqrt{-(p-1)^2}\left(x-\frac{c_2 pt}{p-1}\right)} - \frac{2\sqrt{\kappa_2}(p-1)\cos(p(c_2t+x))}{p} + \mathrm{e}^{\sqrt{-(p-1)^2}\left(\frac{c_2 pt}{p-1}-x\right)}}. \tag{5.27}$$

Set 14:

$$\{c_1 = -\frac{c_2 p}{p-1},\ p_1 = \sqrt{-(p-1)^2},\ \kappa_1 = \frac{2\sqrt{\kappa_2}(p-1)}{p}\}, \tag{5.28}$$

$$u(x,t) = -\frac{2\left(\kappa_2\sqrt{-(p-1)^2}\mathrm{e}^{\sqrt{-(p-1)^2}\left(x-\frac{c_2 pt}{p-1}\right)} - 2\sqrt{\kappa_2}(p-1)\sin\left(p\left(c_2 t+x\right)\right) + \sqrt{-(p-1)^2}\left(-\mathrm{e}^{\sqrt{-(p-1)^2}\left(\frac{c_2 pt}{p-1}-x\right)}\right)\right)}{\kappa_2\mathrm{e}^{\sqrt{-(p-1)^2}\left(x-\frac{c_2 pt}{p-1}\right)} + \frac{2\sqrt{\kappa_2}(p-1)\cos(p(c_2 t+x))}{p} + \mathrm{e}^{\sqrt{-(p-1)^2}\left(\frac{c_2 pt}{p-1}-x\right)}}. \tag{5.29}$$

5.2. Three-wave solution

Consider the relation corresponding to the three-wave solution [38],

$$\begin{cases} \varsigma_1 = a_1 x + d_1 t, \\ \varsigma_2 = a_2 x + d_2 t, \\ \varsigma_3 = a_3 x + d_3 t, \\ f(\zeta) = \kappa_2\mathrm{e}^{\varsigma_1} + \kappa_3\sin\left(\varsigma_3\right) + \kappa_1\cos\left(\varsigma_2\right) + \mathrm{e}^{-(\varsigma_1)}. \end{cases} \tag{5.30}$$

Putting Eq (5.30) into Eq (4.1), we equate the co-efficient of each power of including functions and their products. Adding them equal to zero and resolving the algebraic system, we gain multiple solution sets mentioned as follows:

Set 1:

$$\{a_2 = -\mathrm{i}a_1,\ d_1 = -\mathrm{i}d_2,\ \kappa_1 = -\frac{2\mathrm{i}\left(a_1^2+1\right)\sqrt{\kappa_2}}{\sqrt{-a_1^4-2a_1^2-1}},\ \kappa_3 = 0\}, \tag{5.31}$$

$$u_1(x,t) = -\frac{2\left(a_1\left(\kappa_2\mathrm{e}^{a_1 x+d_1 t} - \frac{2\mathrm{i}\left(a_1^2+1\right)\sqrt{\kappa_2}\sinh(a_1 x+\mathrm{i}d_2 t)}{\sqrt{-\left(a_1^2+1\right)^2}} - \mathrm{e}^{-a_1 x+\mathrm{i}d_2 t}\right)\right)}{\kappa_2\mathrm{e}^{a_1 x+d_1 t} - \frac{2\mathrm{i}\left(a_1^2+1\right)\sqrt{\kappa_2}\cosh(a_1 x+\mathrm{i}d_2 t)}{\sqrt{-\left(a_1^2+1\right)^2}} + \mathrm{e}^{-a_1 x+\mathrm{i}d_2 t}}. \tag{5.32}$$

Set 2:

$$\{a_2 = -\mathrm{i}a_1,\ d_1 = -\mathrm{i}d_2,\ \kappa_1 = \frac{2\mathrm{i}\left(a_1^2+1\right)\sqrt{\kappa_2}}{\sqrt{-a_1^4-2a_1^2-1}},\ \kappa_3 = 0\}, \tag{5.33}$$

$$u(x,t) = -\frac{2\left(a_1\left(\kappa_2\mathrm{e}^{a_1 x-\mathrm{i}d_2 t} + \frac{2\mathrm{i}\left(a_1^2+1\right)\sqrt{\kappa_2}\sinh(a_1 x+\mathrm{i}d_2 t)}{\sqrt{-\left(a_1^2+1\right)^2}} - \mathrm{e}^{-a_1 x+\mathrm{i}d_2 t}\right)\right)}{\kappa_2\mathrm{e}^{a_1 x-\mathrm{i}d_2 t} + \frac{2\mathrm{i}\left(a_1^2+1\right)\sqrt{\kappa_2}\cosh(a_1 x+\mathrm{i}d_2 t)}{\sqrt{-\left(a_1^2+1\right)^2}} + \mathrm{e}^{-a_1 x+\mathrm{i}d_2 t}}. \tag{5.34}$$

Set 3:

$$\{a_2 = \mathrm{i}a_1,\ d_1 = \mathrm{i}d_2,\ \kappa_1 = -\frac{2\mathrm{i}\left(a_1^2+1\right)\sqrt{\kappa_2}}{\sqrt{-a_1^4-2a_1^2-1}},\ \kappa_3 = 0\}, \tag{5.35}$$

$$u(x,t) = -\frac{2\left(a_1\left(\sqrt{-\left(a_1^2+1\right)^2}\kappa_2\mathrm{e}^{2a_1 x+2\mathrm{i}d_2 t} - \mathrm{i}\left(a_1^2+1\right)\sqrt{\kappa_2}\left(\mathrm{e}^{2a_1 x} - e^{2\mathrm{i}d_2 t}\right) - \sqrt{-\left(a_1^2+1\right)^2}\right)\right)}{\sqrt{-\left(a_1^2+1\right)^2}\kappa_2\mathrm{e}^{2a_1 x+2\mathrm{i}d_2 t} - \mathrm{i}\left(a_1^2+1\right)\sqrt{\kappa_2}\left(\mathrm{e}^{2a_1 x} + \mathrm{e}^{2\mathrm{i}d_2 t}\right) + \sqrt{-\left(a_1^2+1\right)^2}}. \tag{5.36}$$

Set 4:

$$\{a_2 = \mathrm{i}a_1,\ d_1 = \mathrm{i}d_2,\ \kappa_1 = \frac{2\mathrm{i}\left(a_1^2+1\right)\sqrt{\kappa_2}}{\sqrt{-a_1^4-2a_1^2-1}},\ \kappa_3 = 0\}, \tag{5.37}$$

$$u(x,t) = -\frac{2\left(a_1\left(\sqrt{-\left(a_1^2+1\right)^2}\kappa_2\mathrm{e}^{2a_1x+2\mathrm{i}d_2t} + \mathrm{i}\left(a_1^2+1\right)\sqrt{\kappa_2}\left(\mathrm{e}^{2a_1x}-\mathrm{e}^{2\mathrm{i}d_2t}\right) - \sqrt{-\left(a_1^2+1\right)^2}\right)\right)}{\sqrt{-\left(a_1^2+1\right)^2}\kappa_2\mathrm{e}^{2a_1x+2\mathrm{i}d_2t} + \mathrm{i}\left(a_1^2+1\right)\sqrt{\kappa_2}\left(\mathrm{e}^{2a_1x}+\mathrm{e}^{2\mathrm{i}d_2t}\right) + \sqrt{-\left(a_1^2+1\right)^2}}. \tag{5.38}$$

Set 5:

$$\{a_2 = -\mathrm{i}\left(a_1-\mathrm{i}\right),\ d_1 = -\mathrm{i}d_2,\ \kappa_1 = -\frac{2a_1\left(a_1+\mathrm{i}\right)\sqrt{\kappa_2}}{\sqrt{a_1^4+2a_1^2+1}},\ \kappa_3 = 0\}, \tag{5.39}$$

$$u(x,t) = -\frac{2a_1\left(\kappa_2\mathrm{e}^{a_1x-\mathrm{i}d_2t} + \frac{2\mathrm{i}\sqrt{\left(a_1^2+1\right)^2}\sqrt{\kappa_2}\sin(\mathrm{i}a_1x-d_2t+x)}{a_1^2+1} - \mathrm{e}^{-a_1x+\mathrm{i}d_2t}\right)}{\kappa_2\mathrm{e}^{a_1x-\mathrm{i}d_2t} - \frac{2a_1(a_1+\mathrm{i})\sqrt{\kappa_2}\cos(\mathrm{i}a_1x-d_2t+x)}{\sqrt{(a_1^2+1)^2}} + \mathrm{e}^{-a_1x+\mathrm{i}d_2t}}. \tag{5.40}$$

Set 6:

$$\{a_2 = -\mathrm{i}\left(a_1-\mathrm{i}\right),\ d_1 = -\mathrm{i}d_2,\ \kappa_1 = \frac{2a_1\left(a_1+\mathrm{i}\right)\sqrt{\kappa_2}}{\sqrt{a_1^4+2a_1^2+1}},\ \kappa_3 = 0\}, \tag{5.41}$$

$$u(x,t) = -\frac{2a_1\left(\kappa_2\mathrm{e}^{a_1x-\mathrm{i}d_2t} - \frac{2\mathrm{i}\sqrt{\left(a_1^2+1\right)^2}\sqrt{\kappa_2}\sin(\mathrm{i}a_1x-d_2t+x)}{a_1^2+1} - \mathrm{e}^{-a_1x+\mathrm{i}d_2t}\right)}{\kappa_2\mathrm{e}^{a_1x-\mathrm{i}d_2t} + \frac{2a_1(a_1+\mathrm{i})\sqrt{\kappa_2}\cos(\mathrm{i}a_1x-d_2t+x)}{\sqrt{(a_1^2+1)^2}} + \mathrm{e}^{-a_1x+\mathrm{i}d_2t}}. \tag{5.42}$$

Set 7:

$$\{a_2 = \mathrm{i}\left(a_1-\mathrm{i}\right),\ d_1 = \mathrm{i}d_2,\ \kappa_1 = -\frac{2a_1\left(a_1+\mathrm{i}\right)\sqrt{\kappa_2}}{\sqrt{a_1^4+2a_1^2+1}},\ \kappa_3 = 0\}, \tag{5.43}$$

$$u_1(x,t) = -\frac{2\left(a_1\kappa_2\mathrm{e}^{a_1x+\mathrm{i}d_2t} + \frac{2(a_1+\mathrm{i})(1+\mathrm{i}a_1)a_1\sqrt{\kappa_2}\sin(\mathrm{i}a_1x+d_2t+x)}{\sqrt{(a_1^2+1)^2}} + a_1\left(-\mathrm{e}^{a_1(-x)-\mathrm{i}d_2t}\right)\right)}{\kappa_2\mathrm{e}^{a_1x+\mathrm{i}d_2t} - \frac{2a_1(a_1+\mathrm{i})\sqrt{\kappa_2}\cos(\mathrm{i}a_1x+d_2t+x)}{\sqrt{(a_1^2+1)^2}} + \mathrm{e}^{a_1(-x)-\mathrm{i}d_2t}}. \tag{5.44}$$

Set 8:

$$\{a_2 = \mathrm{i}\left(a_1-\mathrm{i}\right),\ d_1 = \mathrm{i}d_2,\ \kappa_1 = \frac{2a_1\left(a_1+\mathrm{i}\right)\sqrt{\kappa_2}}{\sqrt{a_1^4+2a_1^2+1}},\ \kappa_3 = 0\}, \tag{5.45}$$

$$u(x,t) = -\frac{2\left(a_1\kappa_2\mathrm{e}^{a_1x+\mathrm{i}d_2t} - \frac{2(1+\mathrm{i}a_1)(a_1+\mathrm{i})a_1\sqrt{\kappa_2}\sin(\mathrm{i}a_1x+d_2t+x)}{\sqrt{(a_1^2+1)^2}} + a_1\left(-\mathrm{e}^{a_1(-x)-\mathrm{i}d_2t}\right)\right)}{\kappa_2\mathrm{e}^{a_1x+\mathrm{i}d_2t} + \frac{2a_1(a_1+\mathrm{i})\sqrt{\kappa_2}\cos(\mathrm{i}a_1x+d_2t+x)}{\sqrt{(a_1^2+1)^2}} + \mathrm{e}^{a_1(-x)-\mathrm{i}d_2t}}. \tag{5.46}$$

Set 9:

$$\{a_2 = -\mathrm{i}\left(a_1+\mathrm{i}\right),\ d_1 = -\mathrm{i}d_2,\ \kappa_1 = -\frac{2a_1\left(a_1-\mathrm{i}\right)\sqrt{\kappa_2}}{\sqrt{a_1^4+2a_1^2+1}},\ \kappa_3 = 0\}, \tag{5.47}$$

$$u(x,t) = -\frac{2\left(a_1\kappa_2 e^{a_1 x - i d_2 t} + \frac{2(a_1-i)(1+ia_1)a_1\sqrt{\kappa_2}\sin(ia_1 x - d_2 t + x)}{\sqrt{(a_1^2+1)^2}} + a_1\left(-e^{-a_1 x + i d_2 t}\right)\right)}{\kappa_2 e^{a_1 x - i d_2 t} - \frac{2a_1(a_1-i)\sqrt{\kappa_2}\cos(ia_1 x - d_2 t + x)}{\sqrt{(a_1^2+1)^2}} + e^{-a_1 x + i d_2 t}}. \tag{5.48}$$

Set 10:

$$\{a_2 = -i(a_1+i),\ d_1 = -id_2,\ \kappa_1 = \frac{2a_1(a_1-i)\sqrt{\kappa_2}}{\sqrt{a_1^4+2a_1^2+1}},\ \kappa_3 = 0\}, \tag{5.49}$$

$$u(x,t) = -\frac{2\left(a_1\kappa_2 e^{a_1 x - i d_2 t} - \frac{2(1+ia_1)(a_1-i)a_1\sqrt{\kappa_2}\sin(ia_1 x - d_2 t + x)}{\sqrt{(a_1^2+1)^2}} + a_1\left(-e^{-a_1 x + i d_2 t}\right)\right)}{\kappa_2 e^{a_1 x - i d_2 t} + \frac{2a_1(a_1-i)\sqrt{\kappa_2}\cos(ia_1 x - d_2 t + x)}{\sqrt{(a_1^2+1)^2}} + e^{-a_1 x + i d_2 t}}. \tag{5.50}$$

Set 11:

$$\{a_2 = i(a_1+i),\ d_1 = id_2,\ \kappa_1 = -\frac{2a_1(a_1-i)\sqrt{\kappa_2}}{\sqrt{a_1^4+2a_1^2+1}},\ \kappa_3 = 0\}, \tag{5.51}$$

$$u(x,t) = -\frac{2\left(a_1\kappa_2 e^{a_1 x + i d_2 t} + \frac{2(a_1-i)(1+ia_1)a_1\sqrt{\kappa_2}\sin(ia_1 x + d_2 t + x)}{\sqrt{(a_1^2+1)^2}} + a_1\left(-e^{a_1(-x) - i d_2 t}\right)\right)}{\kappa_2 e^{a_1 x + i d_2 t} - \frac{2a_1(a_1-i)\sqrt{\kappa_2}\cos(ia_1 x + d_2 t + x)}{\sqrt{(a_1^2+1)^2}} + e^{a_1(-x) - i d_2 t}}. \tag{5.52}$$

Set 12:

$$\{a_2 = i(a_1+i),\ d_1 = id_2,\ \kappa_1 = \frac{2a_1(a_1-i)\sqrt{\kappa_2}}{\sqrt{a_1^4+2a_1^2+1}},\ \kappa_3 = 0\}, \tag{5.53}$$

$$u(x,t) = -\frac{2\left(a_1\kappa_2 e^{a_1 x + i d_2 t} - \frac{2(1+ia_1)(a_1-i)a_1\sqrt{\kappa_2}\sin(ia_1 x + d_2 t + x)}{\sqrt{(a_1^2+1)^2}} + a_1\left(-e^{a_1(-x) - i d_2 t}\right)\right)}{\kappa_2 e^{a_1 x + i d_2 t} + \frac{2a_1(a_1-i)\sqrt{\kappa_2}\cos(ia_1 x + d_2 t + x)}{\sqrt{(a_1^2+1)^2}} + e^{a_1(-x) - i d_2 t}}. \tag{5.54}$$

6. Graphs

In this section, the corresponding results are presented by selecting appropriate parameter values for the analytical breather-wave and new three-wave solutions. The results are illustrated in the following figures: In Figure 2, we present 3D+contour and 2D plots for Re[u] in panels (a) and (d), Abs[u] in panels (b) and (e), and Im[u] in panels (c) and (f), with the parameters $c_1 = 4.1$ and $\kappa_2 = 0.7$ and the spatial and temporal domains $x \in [-10, 10]$ and $t \in [-2, 2]$. Figure 3 shows similar plots with Re[u] in panels (a) and (d), Abs[u] in panels (b) and (e), and Im[u] in panels (c) and (f) for the parameters $p = 1.1$, $c_2 = 1.7$, and $\kappa_2 = 1.3$, within the same spatial and temporal intervals $x \in [-10, 10]$ and $t \in [-2, 2]$. In Figure 4, the corresponding 3D+contour and 2D plots are shown for Re[u] in panels (a) and (d), Abs[u] in panels (b) and (e), and Im[u] in panels (c) and (f), with the parameters $\kappa_1 = 4.3$, $p = -2.9$, $c_2 = 1.7$, and $\kappa_2 = 4.5$, where $x \in [-2, 2]$ and $t \in [-2, 2]$. Figure 5 illustrates similar plots for the parameters $a_1 = -0.5$, $d_2 = 0.7$, and $\kappa_2 = 2$, with spatial and temporal domains $x \in [-10, 10]$ and $t \in [-5, 5]$. Finally, in Figure 6, the 3D+contour and 2D plots for Re[u]

in panels (a) and (d), Abs[u] in panels (b) and (e), and Im[u] in panels (c) and (f) are presented with the parameters $a_1 = 1.2$, $d_2 = -1.2$, and $\kappa_2 = -3.8$, with $x \in [-5, 5]$ and $t \in [-5, 5]$. Overall, these visualizations not only confirm the validity of the derived analytical solutions but also provide a comprehensive understanding of their localized structures, wave dynamics, energy exchange, and long-term behaviors under various parameter regimes. The obtained analytical solutions are useful for understanding nonlinear wave propagation in physical media and can model pulse transmission in optical fibers, surface wave propagation in shallow water, and nonlinear structures in plasma.

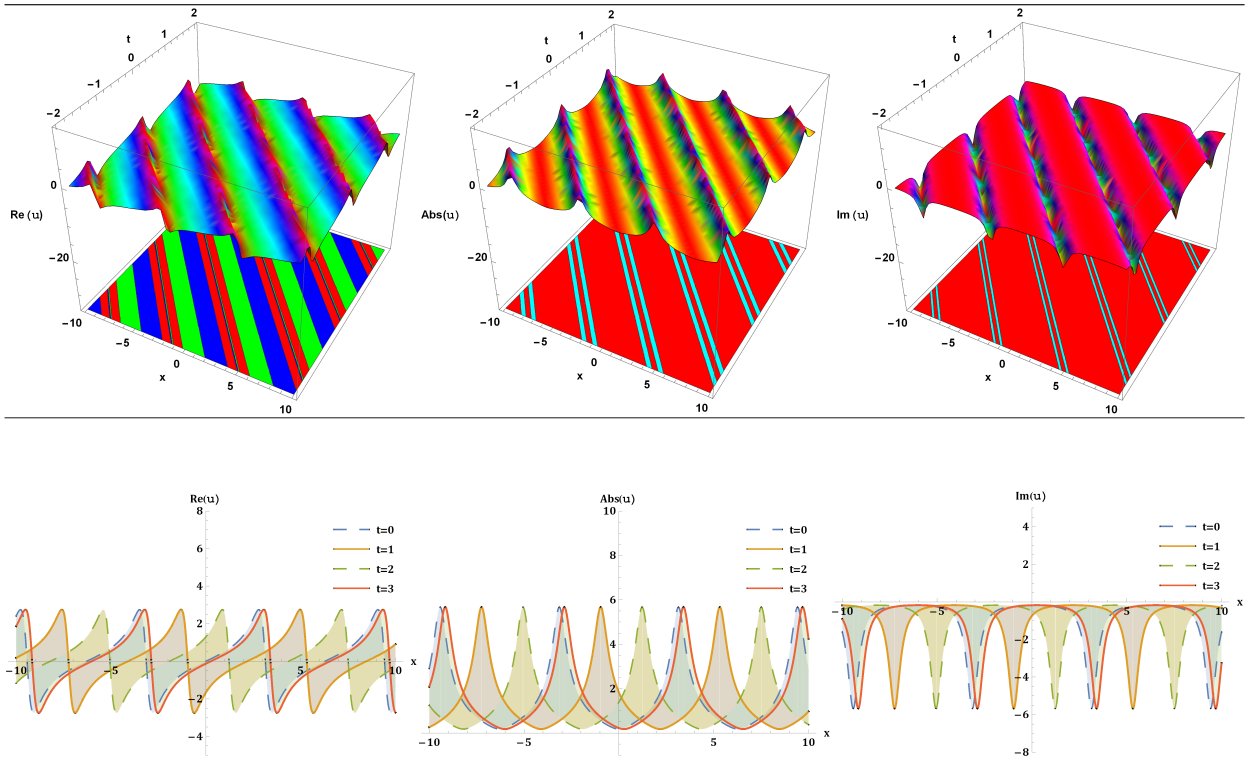

Figure 2. Breather-wave solution described in Eq (5.3) in 3D+contour and 2D with Re[u], Abs[u], and Im[u] graphs.

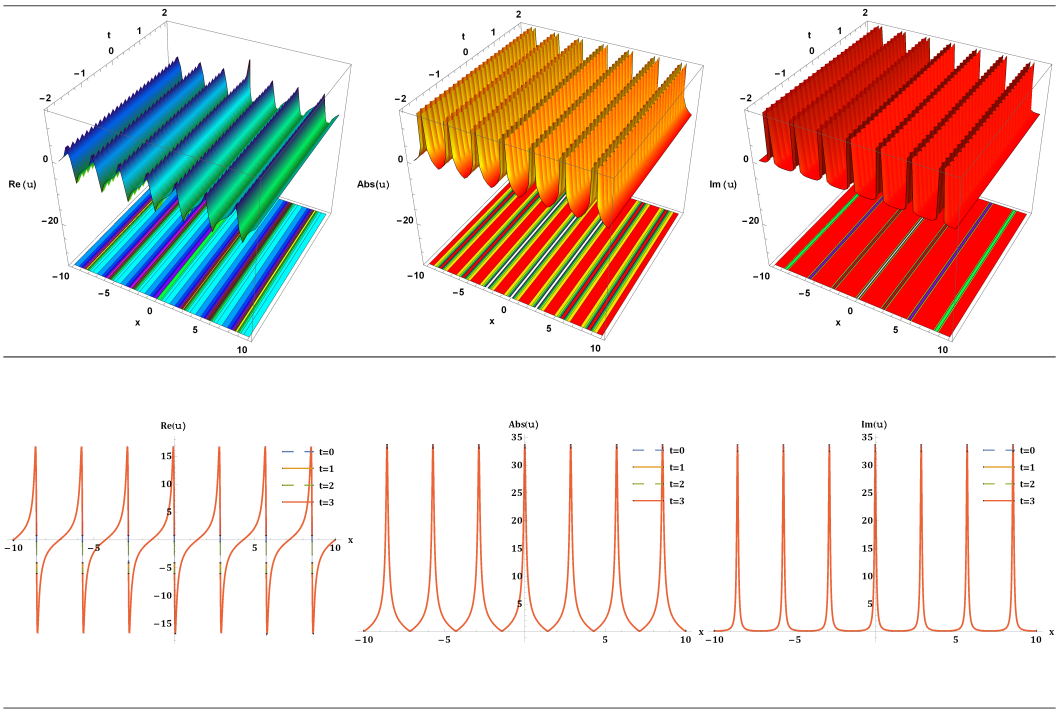

Figure 3. Breather-wave solution described in Eq (5.7) in 3D+contour and 2D with Re[u], Abs[u], and Im[u] graphs.

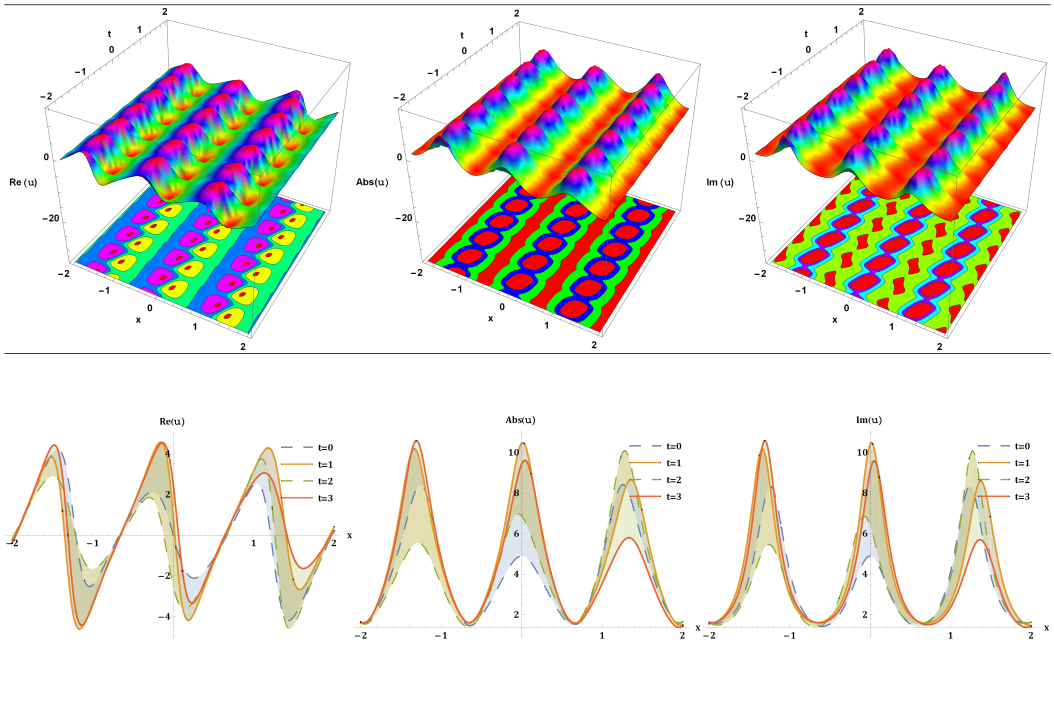

Figure 4. Breather-wave solution described in Eq (5.15) in 3D+contour and 2D with Re[u], Abs[u], and Im[u] graphs.

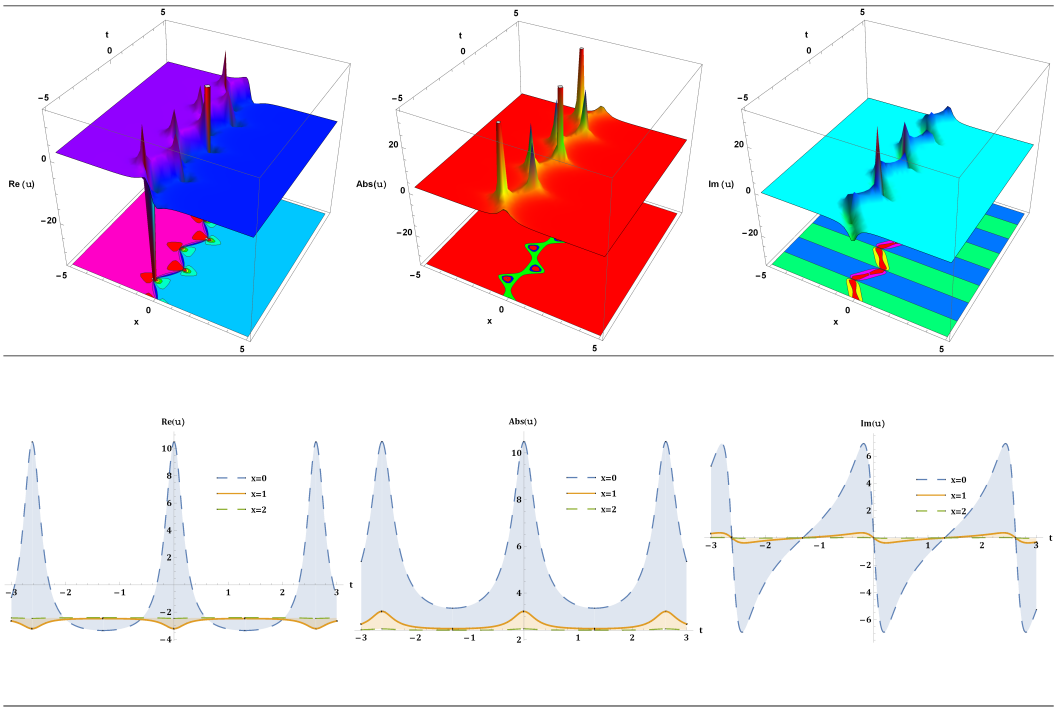

Figure 5. New three-wave solution described in Eq (5.36) in 3D+contour and 2D with Re[u], Abs[u], and Im[u] graphs.

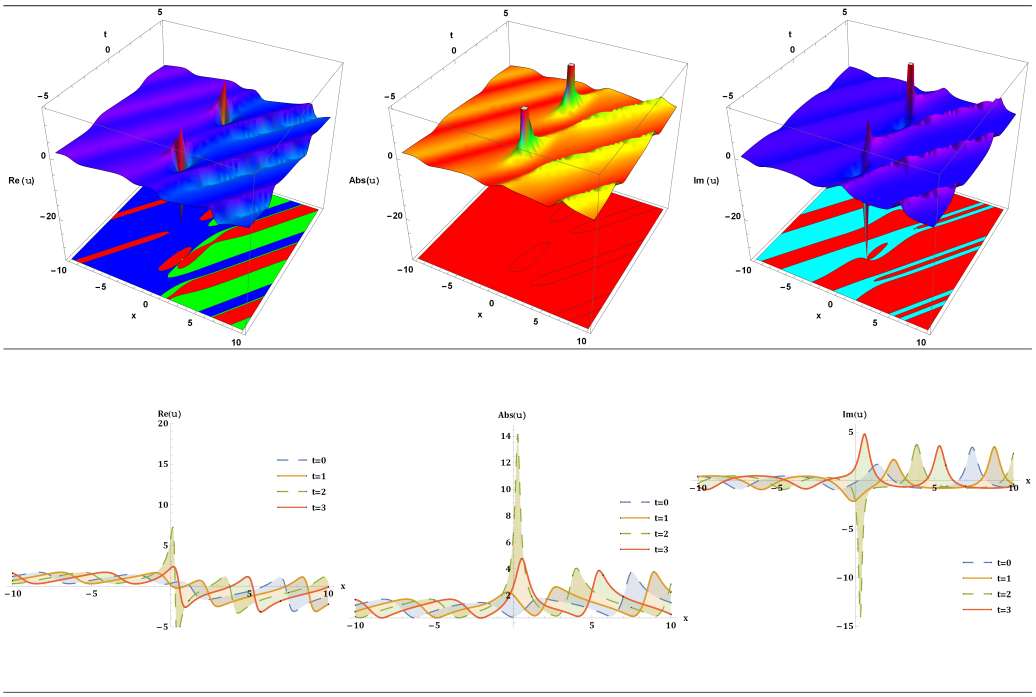

Figure 6. New three-wave solution described in Eq (5.40) in 3D+contour and 2D with Re[u], Abs[u], and Im[u] graphs.

7. Machine learning

In this work, we utilize the MLP regressor algorithm, which consists of an input layer, an output layer, and one or more hidden layers [39]. The structure of the network is defined by the following equation for the output of the first hidden layer:

$$\hat{y}^{(1)} = \varphi^{(1)}\left(\sum_{i=1}^{q^{(l-1)}} w_{ij}^{(l)}\hat{y}_i^{(l-1)} + b_j^{(l)}\right), \tag{7.1}$$

where

- $\hat{y}^{(1)}$: Output of the first layer.
- $\varphi^{(1)}$: Activation function applied to the hidden layer.
- $q^{(l-1)}$: Number of neurons in the $(l-1)^{\text{th}}$ layer.
- $w_{ij}^{(l)}$: Weight connecting the i^{th} neuron in layer $(l-1)$ to the j^{th} neuron in layer l.
- $\hat{y}_i^{(l-1)}$: Output of the i^{th} neuron in the $(l-1)^{\text{th}}$ layer.
- $b_j^{(l)}$: Bias term for the j^{th} neuron in layer l.

The activation function is defined as

$$\varphi_j(x) = \frac{1}{1+\mathrm{e}^{-y_j(x)}}, \tag{7.2}$$

and the performance of the model is assessed using the mean squared error (MSE) metric:

$$\text{MSE} = \sqrt{\frac{1}{n}\sum_{i=1}^{n}(y_i - x_i)^2}. \tag{7.3}$$

The data set is partitioned into 80% for training and 20% for testing, with normalization applied to scale all data within the range $[0, 1]$. The NN framework and training strategy are summarized as follows:

- **Data normalization:** Inputs are scaled to lie within $[0, 1]$.
- **Network architecture:** The NN consists of an input layer, multiple hidden layers, and an output layer.
- **Computation flow:** Forward and backward propagation are carried out using the sigmoid activation function.
- **Optimization:** Parameters are updated using the gradient descent algorithm.
- **Error function:** The MSE is used to measure deviations between predicted and actual outputs.
- **Learning rate:** Fixed at $\eta = 0.1$.
- **Training iterations:** The model is trained for 10,000 and 100,000 iterations to achieve higher accuracy.
- **Implementation:** Simulations are performed in Python 3.13.1.

The resulting plots display the behavior of the actual versus predicted outputs, as well as the error curves for different training durations.

8. Results and discussion

We present two example solutions to demonstrate the prediction capability of the machine learning algorithm. Although only these two are discussed here, the same procedure can be applied to the remaining solutions.

- **Case 1: Solution Eq** (5.15)

  - Figure 7 shows the wave dynamics of the solution using both actual and predicted data.
  - The MLP regressor provides predictions closely matching the results shown in Figure 4.
  - The model was trained for 10,000 epochs.
  - The MSE between actual and predicted data, representing the error, is reported in Table 1.

Table 1. Epochs and error while performing the prediction of the solution given by Eq (5.15).

For Re[u] solution										
Epoch	1000	2000	3000	4000	5000	6000	7000	8000	9000	10000
Error	0.0003	0.0000	0.0000	0.0000	0.0000	0.0000	0.0000	0.0000	0.0000	0.0000
For Abs[u] solution										
Epoch	1000	2000	3000	4000	5000	6000	7000	8000	9000	10000
Error	0.0001	0.0000	0.0000	0.0000	0.0000	0.0000	0.0000	0.0000	0.0000	0.0000
For Im[u] solution										
Epoch	1000	2000	3000	4000	5000	6000	7000	8000	9000	10000
Error	0.0002	0.0000	0.0000	0.0000	0.0000	0.0000	0.0000	0.0000	0.0000	0.0000

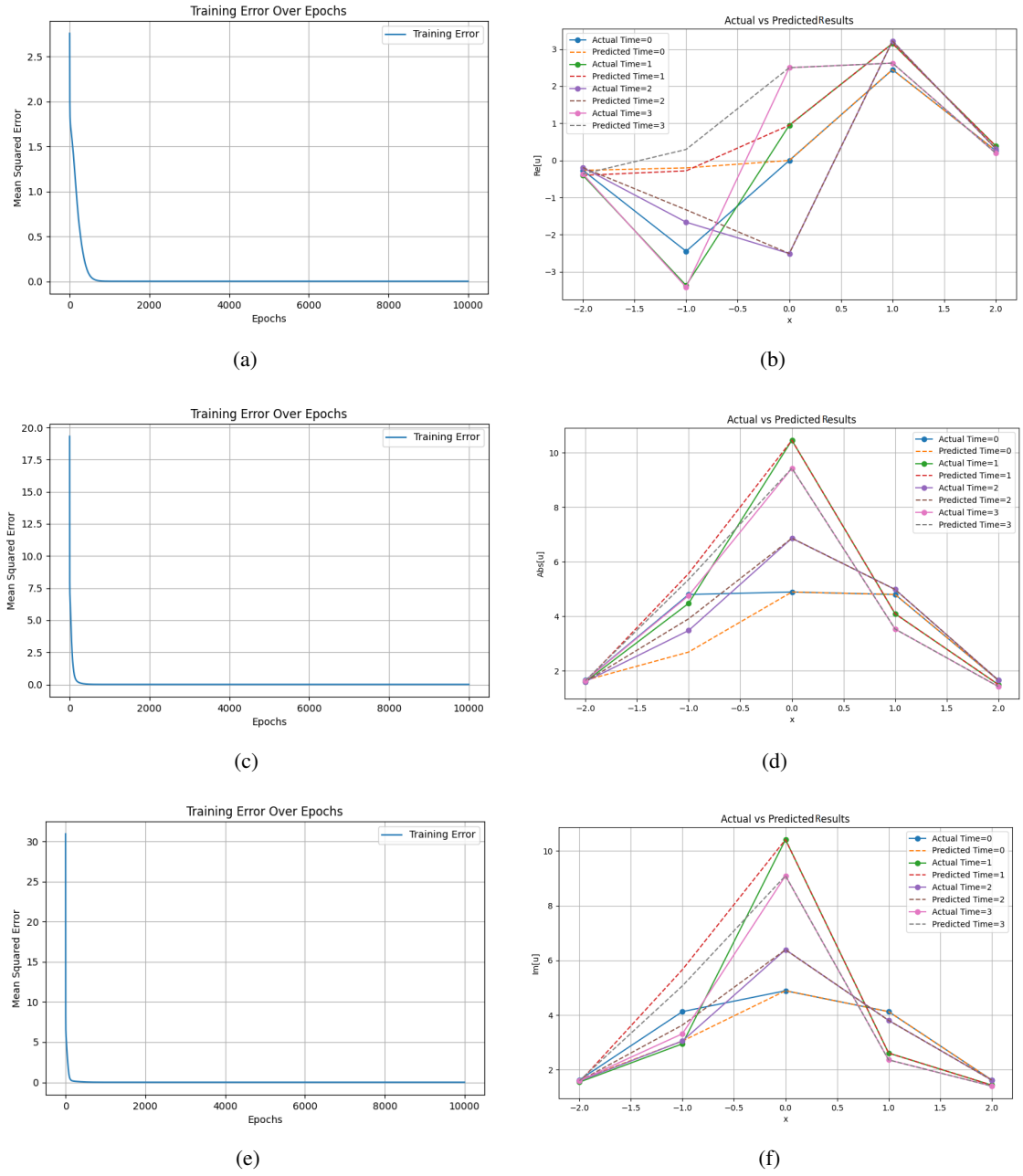

Figure 7. Actual and predicted wave dynamics of the solution described by Eq (5.15).

- **Case 2: Solution Eq** (5.36)
  - Figure 8 shows the wave dynamics of the solution using both actual and predicted data.
  - The MLP regressor provides predictions closely matching the results shown in Figure 5.
  - The model was trained for 100,000 epochs.
  - The MSE between actual and predicted data, representing the error, is reported in Table 2.

These cases demonstrate that the MLP regressor shows less error when it has more data and training epochs, resulting in more accurate predictions.

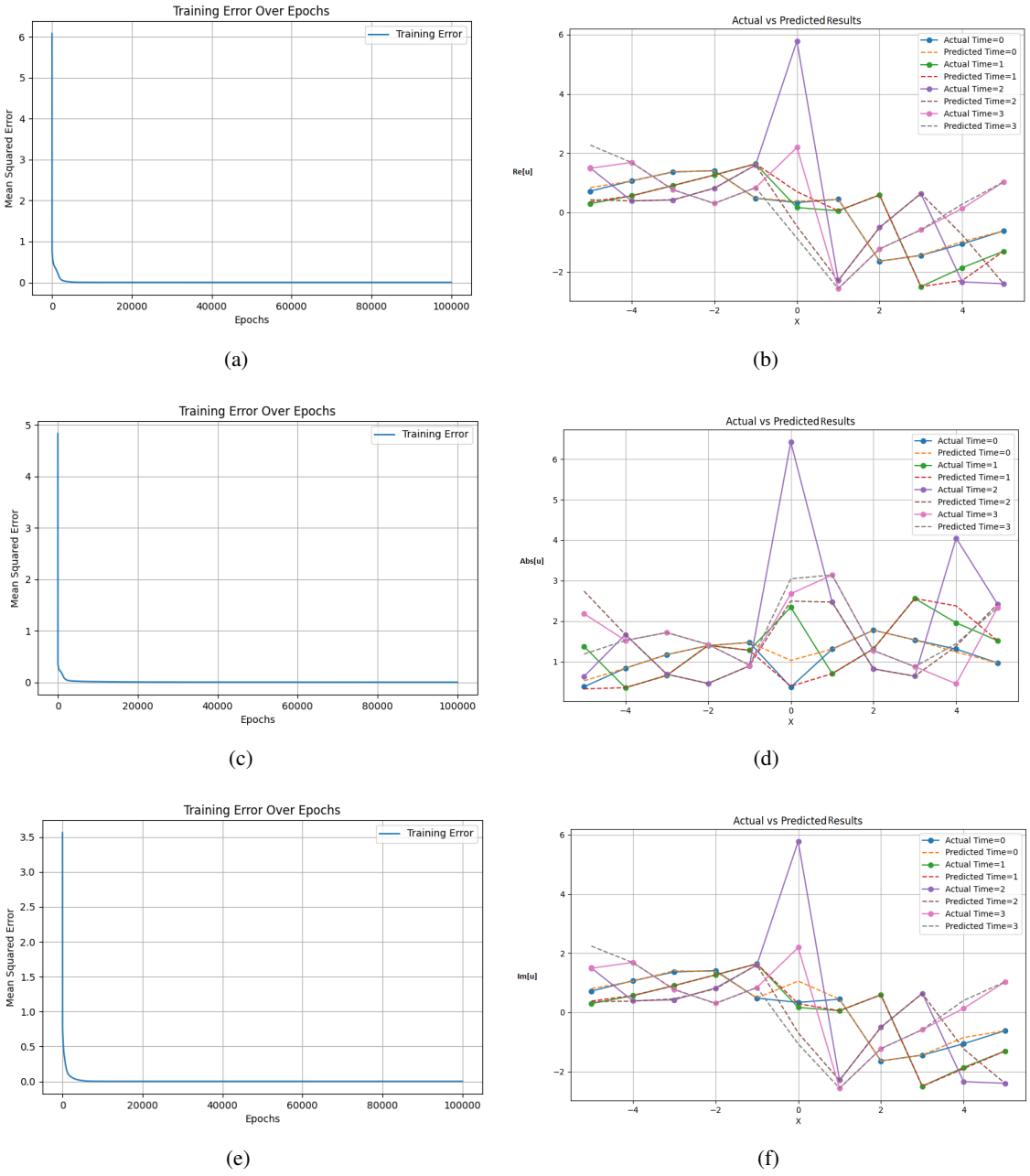

Figure 8. Actual and predicted wave dynamics of the solution described by Eq (5.36).

Table 2. Epochs and error while performing the prediction of the solution given by Eq (5.36).

For Re[u] solution										
Epoch	10000	20000	30000	40000	50000	60000	70000	80000	90000	100000
Error	0.0004	0.0001	0.0001	0.0001	0.0001	0.0000	0.0000	0.0000	0.0000	0.0000
For Abs[u] solution										
Epoch	10000	20000	30000	40000	50000	60000	70000	80000	90000	100000
Error	0.0033	0.0019	0.0002	0.0000	0.0000	0.0000	0.0000	0.0000	0.0000	0.0000
For Im[u] solution										
Epoch	10000	20000	30000	40000	50000	60000	70000	80000	90000	100000
Error	0.0003	0.0002	0.0002	0.0002	0.0002	0.0002	0.0002	0.0002	0.0002	0.0002

8.1. Comparison

Compared to previous studies, the present work derives explicit three-wave interaction and breather-wave solutions of the Kairat-II equation, revealing localized and oscillatory behaviors not reported before. In addition, the application of a machine learning framework (MLP regressor) to predict soliton dynamics provides a modern computational perspective that complements the analytical solutions. The asymptotic analysis further characterizes the long-term behavior of these solutions, collectively highlighting the novelty and significance of the proposed methodology.

9. Asymptotic analysis on the soliton solutions

This section consists of the asymptotic behavior of the gained soliton solutions. Here, we apply the breather and three-wave soliton solutions. First, we apply the breather wave Eq (5.3) solution.
Case 1: If $x \to \pm\infty$ **at** $t = 0$**,**

$$u(x,0) = -\frac{\mathrm{i}\left(1-\kappa_2 \mathrm{e}^{\mathrm{i}(x)}\right)}{1+\kappa_2 \mathrm{e}^{\mathrm{i}(x)}}. \tag{9.1}$$

Case 2: If $t \to \pm\infty$ **at** $x = 0$**,**

$$u(0,t) = -\frac{\mathrm{i}\left(1-\kappa_2 \mathrm{e}^{\mathrm{i}(c_1 t)}\right)}{1+\kappa_2 \mathrm{e}^{\mathrm{i}(c_1 t)}}. \tag{9.2}$$

Figures 9 and 10 show the asymptotic behavior of Eqs (9.1) and (9.2), respectively.

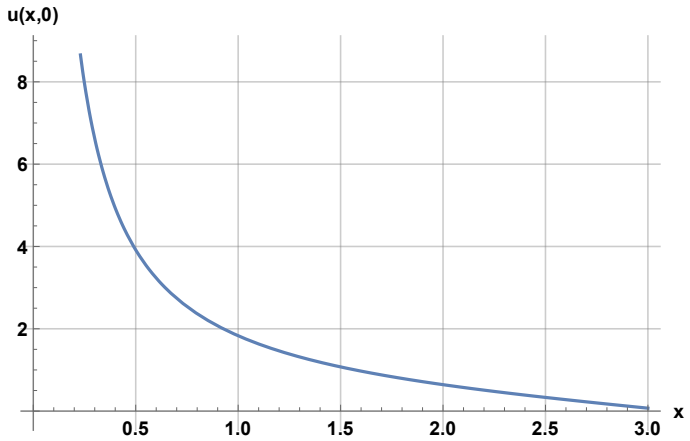

Figure 9. Asymptotic behavior of Eq (9.1).

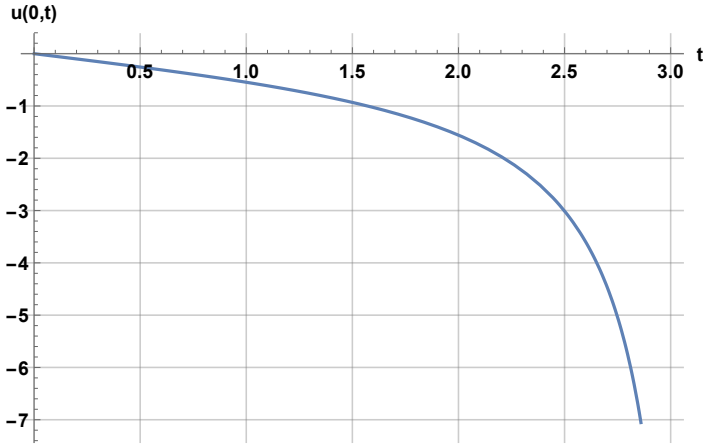

Figure 10. Asymptotic behavior of Eq (9.2).

Now we apply the three-wave Eq (5.32) solution.

Case 1: If $x \to \pm\infty$ **at** $t = 0$**,**

$$u(x,0) = -\frac{2\left(a_1\left(\kappa_2 e^{a_1 x} - \frac{2i\left(a_1^2+1\right)\sqrt{\kappa_2}\sinh(a_1 x)}{\sqrt{-\left(a_1^2+1\right)^2}} - e^{-a_1 x}\right)\right)}{\kappa_2 e^{a_1 x} - \frac{2i\left(a_1^2+1\right)\sqrt{\kappa_2}\cosh(a_1 x)}{\sqrt{-\left(a_1^2+1\right)^2}} + e^{-a_1 x}}. \tag{9.3}$$

Case 2: If $t \to \pm\infty$ **at** $x = 0$**,**

$$u(0,t) = -\frac{2\left(a_1\left(\kappa_2 e^{d_1 t} - \frac{2i\left(a_1^2+1\right)\sqrt{\kappa_2}\sinh(id_2 t)}{\sqrt{-\left(a_1^2+1\right)^2}} - e^{id_2 t}\right)\right)}{\kappa_2 e^{d_1 t} - \frac{2i\left(a_1^2+1\right)\sqrt{\kappa_2}\cosh(id_2 t)}{\sqrt{-\left(a_1^2+1\right)^2}} + e^{id_2 t}}. \tag{9.4}$$

Figures 11 and 12 show the asymptotic behavior of Eqs (9.3) and (9.4), respectively.

•**Advantages:**

- Focus on dominant terms and ignoring smaller effects.

- Useful in stability analysis and optimization.
- E.g., approximations in physics, engineering.

• **Disadvantages:**

- Might miss transient or finite-size effects.
- Not always true for complex systems.
- E.g., in systems with multiple scales.

•**Asymptotic behavior has many applications:**

- Algorithm analysis: Understanding time/space complexity.
- Physics: Approximating limits in mechanics, thermodynamics, or quantum systems.
- Biology: Modeling population growth or disease spread.
- Finance: Analyzing long-term investment trends or option pricing.
- Control systems: Assessing stability and performance limits.

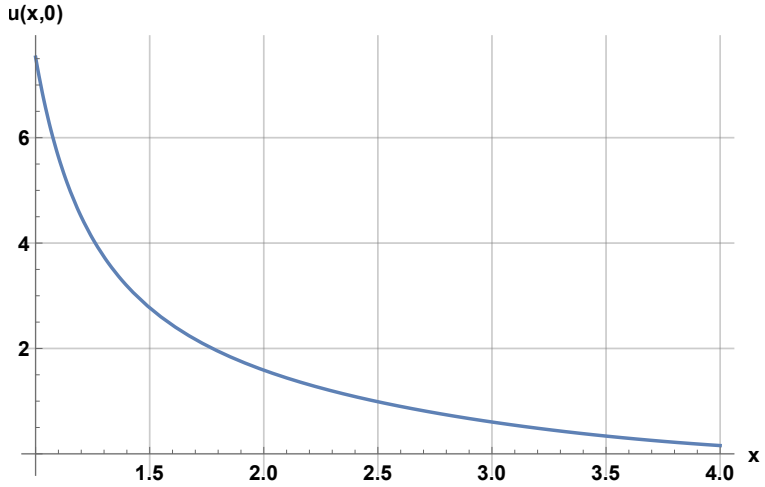

Figure 11. Asymptotic behavior of Eq (9.3).

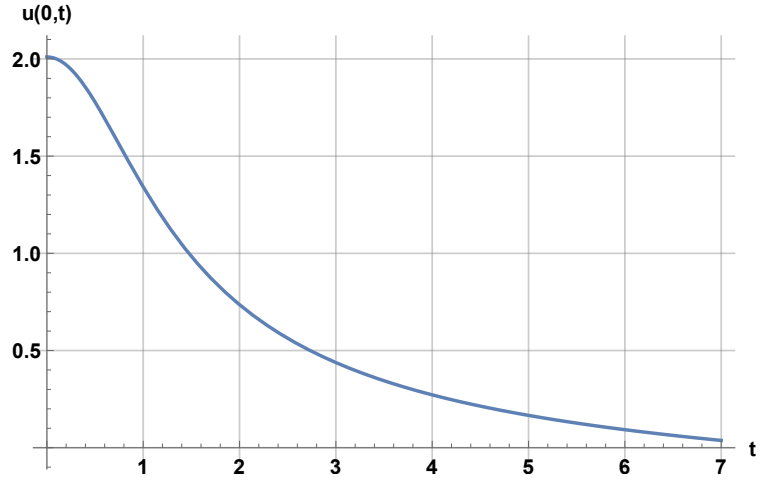

Figure 12. Asymptotic behavior of Eq (9.4).

10. Conclusions

In this work, the integrability of the Kairat-II equation was examined using Painlevé analysis, which confirmed that the model satisfies the Painlevé property. This result supports the mathematical consistency of the equation and highlights its potential for admitting exact analytical solutions, thereby motivating further analytical investigations. By employing Hirota's trilinear method, novel three-wave and breather-wave solutions were successfully derived. In addition, a machine learning framework based on the MLP regressor algorithm was implemented to predict the dynamical behavior of the obtained soliton solutions. The agreement between analytical and predicted results was verified through graphical comparisons using Mathematica and Python. The visualizations, including 2D plots, 3D surface profiles, and contour maps, provided a comprehensive illustration of the wave dynamics. Furthermore, asymptotic analysis was carried out to investigate the long-distance and long-time behavior of the derived solutions. This analysis clarified the localization and propagation characteristics of the waves and confirmed the physical relevance of the obtained structures. The findings of this study have potential applications in areas such as nonlinear optics, plasma physics, and fluid dynamics, where nonlinear wave propagation and interactions play a significant role. The combination of confirmed integrability, exact soliton solutions, asymptotic behavior, and machine learning-based prediction offers a reliable framework for understanding complex nonlinear wave phenomena. Moreover, the proposed computational approach can be extended to other NPDE models. Overall, the results presented here provide new insights into the structure and dynamics of the Kairat-II equation and contribute to the broader study of nonlinear evolution equations.

Author contributions

Waseem Razzaq, Asim Zafar, Naif Almusallam, Fawaz Khaled Alarfaj: Concept, methodology, investigation, formal analysis, visualization, writing–review, funding. All authors of this article have been contributed equally. All authors have read and approved the final version of the manuscript for publication.

Use of Generative-AI tools declaration

The authors declare they have not used Artificial Intelligence (AI) tools in the creation of this article.

Funding

This work was funded by the Deanship of Scientific Research, Vice Presidency for Graduate Studies and Scientific Research, King Faisal University, Saudi Arabia [Grant No. KFU261255].

Conflicts of interest

All authors declare no conflicts of interest in this paper.

References

1. S. Behera, Analytical solutions of fractional order Newell–Whitehead–Segel equation, In: *Modeling, analysis and simulations of multiscale transport phenomena. ICMASMTP 2022*, Singapore: Springer, 2025, 207–221. https://doi.org/10.1007/978-981-96-3098-1_15
2. D. O'Regan, S. R. Aderyani, R. Saadati, M. Inc, Soliton solution of the nonlinear time fractional equations: Comprehensive methods to solve physical models, *Axioms*, **13** (2024), 92. https://doi.org/10.3390/axioms13020092
3. E. M. Ozkan, O. Yildirim, A. Ozkan, On the exact solutions of optical perturbed fractional Schrödinger equation, *Phys. Scr.*, **98** (2023), 115104. https://doi.org/10.1088/1402-4896/acfa2f
4. K. K. Ali, A. Zafar, W. Razzaq, H. Ahmad, F. A. Awwad, E. A. A. Ismail, The kink solitary wave and numerical solutions for conformable nonlinear space–time fractional differential equations, *Results Phys.*, **58** (2024), 107423. https://doi.org/10.1016/j.rinp.2024.107423
5. H. Qawaqneh, A. Zafar, M. Raheel, A. A. Zaagan, E. H. M. Zahran, A. Cevikel, et al., New soliton solutions of M-fractional Westervelt model in ultrasound imaging via two analytical techniques, *Opt. Quant. Electron.*, **56** (2024), 737. https://doi.org/10.1007/s11082-024-06371-1
6. K. S. Nisar, A. Ciancio, K. K. Ali, M. S. Osman, C. Cattani, D. Baleanu, et al., On beta-time fractional biological population model with abundant solitary wave structures, *Alex. Eng. J.*, **61** (2022), 1996–2008. https://doi.org/10.1016/j.aej.2021.06.106
7. W. Razzaq, A. Zafar, A. Akbulut, Applications of the simplest equation procedure to some fractional order differential equations in mathematical physics, *Int. J. Appl. Comput. Math.*, **10** (2024), 56. https://doi.org/10.1007/s40819-024-01687-8
8. B. Hong, Abundant explicit solutions for the M-fractional coupled nonlinear Schrödinger–KdV equations, *J. Low Freq. Noise Vib. Act. Control*, **42** (2023), 1222–1241. https://doi.org/10.1177/14613484221148411
9. R. Kumar, K. S. Pandey, A. Kumar, A. Kumar, Novel traveling wave solutions of Jaulent–Miodek equations and coupled Konno–Oono systems and their dynamics, *Chaos Theory Appl.*, **5** (2023), 281–285. https://doi.org/10.51537/chaos.1322939
10. A. A. Mahmud, K. A. Muhamad, T. Tanriverdi, H. M. Baskonus, An investigation of Fokas system using two new modifications for the trigonometric and hyperbolic trigonometric function methods, *Opt. Quant. Electron.*, **56** (2024), 717. https://doi.org/10.1007/s11082-024-06388-6
11. A. H. Abdel-Aty, S. Arshed, N. Raza, T. A. Alrebdi, K. S. Nisar, H. Eleuch, Investigation of complex hyperbolic and periodic wave structures to a new form of the q-deformed sinh-Gordon equation with fractional temporal evolution, *AIP Adv.*, **14** (2024), 025231. https://doi.org/10.1063/5.0191869
12. S. Albosaily, E. M. Elsayed, M. D. Albalwi, M. Alesemi, W. W. Mohammed, The analytical stochastic solutions for the stochastic potential Yu–Toda–Sasa–Fukuyama equation with conformable derivative using different methods, *Fractal Fract.*, **7** (2023), 787. https://doi.org/10.3390/fractalfract7110787
13. Y. Qi, Y. Tian, Y. Jiang, Existence of traveling wave solutions for the perturbed modified Gardner equation, *Qual. Theory Dyn. Syst.*, **23** (2024), 106. https://doi.org/10.1007/s12346-024-00960-x

14. M. N. Rafiq, M. H. Rafiq, H. Alsaud, Diversity of soliton dynamics, positive multi-complexiton solutions and modulation instability for (3+1)-dimensional extended Kairat-X equation, *Mod. Phys. Lett. B*, **39** (2025), 2550112. https://doi.org/10.1142/S021798492550112X
15. Y. Bo, D. Tian, X. Liu, Y. Jin, Discrete maximum principle and energy stability of the compact difference scheme for two-dimensional Allen-Cahn equation, *J. Funct. Spaces*, **2022** (2022), 8522231. https://doi.org/10.1155/2022/8522231
16. Z. Myrzakulova, S. Manukure, R. Myrzakulov, G. Nugmanova, Integrability, geometry and wave solutions of some Kairat equations, *arXiv:2307.00027*, 2023. https://arxiv.org/abs/2307.00027
17. W. A. Faridi, A. M. Wazwaz, A. M. Mostafa, R. Myrzakulov, Z. Umurzakhova, The Lie point symmetry criteria and formation of exact analytical solutions for Kairat-II equation: Paul–Painlevé approach, *Chaos Solitons Fract.*, **182** (2024), 114745. https://doi.org/10.1016/j.chaos.2024.114745
18. W. A. Faridi, G. H. Tipu, Z. Myrzakulova, R. Myrzakulov, S. A. AlQahtani, P. Pathak, The sensitivity demonstration and propagation of hyper-geometric soliton waves in plasma physics of Kairat-II equation, *Phys. Scr.*, **99** (2024), 045209. https://doi.org/10.1088/1402-4896/ad2bc2
19. M. Awadalla, A. Zafar, A. Taishiyeva, M. Raheel, R. Myrzakulov, A. Bekir, The analytical solutions to the M-fractional Kairat-II and Kairat-X equations, *Front. Phys.*, **11** (2023), 1335423. https://doi.org/10.3389/fphy.2023.1335423
20. J. Muhammad, S. U. Rehman, N. Nasreen, M. Bilal, U. Younas, Exploring the fractional effect to the optical wave propagation for the extended Kairat-II equation, *Nonlinear Dyn.*, **113** (2025), 1501–1512. https://doi.org/10.1007/s11071-024-10139-3
21. A. M. Wazwaz, Extended (3+1)-dimensional Kairat-II and Kairat-X equations: Painlevé integrability, multiple soliton solutions, lump solutions, and breather wave solutions, *Int. J. Numer. Methods Heat Fluid Flow*, **34** (2024), 2177–2194. https://doi.org/10.1108/HFF-01-2024-0053
22. M. Raheel, M. Inc, E. Tala-Tebue, K. H. Mahmoud, Breather, kink and rogue wave solutions of Sharma–Tasso–Olver-like equation, *Opt. Quant. Electron.*, **54** (2022), 560. https://doi.org/10.1007/s11082-022-03933-z
23. A. Zafar, M. Raheel, H. Rezazadeh, M. Inc, M. A. Akinlar, New chirp-free and chirped form optical solitons to the nonlinear Schrödinger equation, *Opt. Quant. Electron.*, **53** (2021), 604. https://doi.org/10.1007/s11082-021-03254-7
24. T. Mathanaranjan, New optical solitons and modulation instability analysis of generalized coupled nonlinear Schrödinger–KdV system, *Opt. Quant. Electron.*, **54** (2022), 336. https://doi.org/10.1007/s11082-022-03723-7
25. N. Raza, A. R. Seadawy, S. Arshed, M. H. Rafiq, A variety of soliton solutions for the Mikhailov–Novikov–Wang dynamical equation via three analytical methods, *J. Geom. Phys.*, **176** (2022), 104515. https://doi.org/10.1016/j.geomphys.2022.104515
26. S. Akçağı, T. Aydemir, Comparison between the (G'/G)-expansion method and the modified extended tanh method, *Open Phys.*, **14** (2016), 88–94. https://doi.org/10.1515/phys-2016-0006
27. A. Zafar, A. Bekir, M. Raheel, H. Rezazadeh, Investigation for optical soliton solutions of two nonlinear Schrödinger equations via two concrete finite series methods, *Int. J. Appl. Comput. Math.*, **6** (2020), 65. https://doi.org/10.1007/s40819-020-00818-1

28. Z. Chen, J. Manafian, M. Raheel, A. Zafar, F. Alsaikhan, M. Abotaleb, Extracting the exact solitons of time-fractional three coupled nonlinear Maccari's system with complex form via four different methods, *Results Phys.*, **36** (2022), 105400. https://doi.org/10.1016/j.rinp.2022.105400
29. J. Manafian, Variety interaction solutions comprising lump solitons for a generalized BK equation by trilinear analysis, *Eur. Phys. J. Plus*, **136** (2021), 1097. https://doi.org/10.1140/epjp/s13360-021-02065-9
30. L. Cheng, Y. Zhang, W. X. Ma, Wronskian N-soliton solutions to a generalized KdV equation in (2+1)-dimensions, *Nonlinear Dyn.*, **111** (2023), 1701–1714. https://doi.org/10.1007/s11071-022-07920-7
31. L. Cheng, Y. Zhang, W. X. Ma, J. Y. Ge, Wronskian and lump wave solutions to an extended second KP equation, *Math. Comput. Simul.*, **187** (2021), 720–731. https://doi.org/10.1016/j.matcom.2021.03.024
32. H. F. Ismael, H. Bulut, Nonlinear dynamics of (2+1)-dimensional Bogoyavlenskii–Schieff equation arising in plasma physics, *Math. Methods Appl. Sci.*, **44** (2021), 10321–10330. https://doi.org/10.1002/mma.7409
33. C. Wang, Z. Dai, Dynamic behaviors of bright and dark rogue waves for the (2+1)-dimensional Nizhnik–Novikov–Veselov equation, *Phys. Scr.*, **90** (2015), 065205. https://doi.org/10.1088/0031-8949/90/6/065205
34. T. Y. Zhou, B. Tian, Y. Q. Chen, Y. Shen, Painlevé analysis, auto-Bäcklund transformation and analytic solutions of a (2+1)-dimensional generalized Burgers system with variable coefficients in a fluid, *Nonlinear Dyn.*, **108** (2022), 2417–2428. https://doi.org/10.1007/s11071-022-07211-1
35. S. Singh, S. S. Ray, Painlevé analysis, auto-Bäcklund transformation and new exact solutions of (2+1) and (3+1)-dimensional extended Sakovich equation with time dependent variable coefficients in ocean physics, *J. Ocean Eng. Sci.*, **8** (2023), 246–262. https://doi.org/10.1016/j.joes.2022.01.008
36. B. Mohan, S. Kumar, R. Kumar, Higher-order rogue waves and dispersive solitons of a novel P-type (3+1)-D evolution equation in soliton theory and nonlinear waves, *Nonlinear Dyn.*, **111** (2023), 20275–20288. https://doi.org/10.1007/s11071-023-08938-1
37. W. Razzaq, A. Zafar, Bilinearization of generalized Bogoyavlensky–Konopelchenko equation with neural networks: Painlevé analysis, *Nonlinear Dyn.*, **113** (2025), 25083–25096. https://doi.org/10.1007/s11071-025-11384-w
38. J. G. Liu, J. Q. Du, Z. F. Zeng, B. Nie, New three-wave solutions for the (3+1)-dimensional Boiti–Leon–Manna–Pempinelli equation, *Nonlinear Dyn.*, **88** (2017), 655–661. https://doi.org/10.1007/s11071-016-3267-2
39. W. Razzaq, A. Zafar, Machine learning-enhanced soliton solutions for the Lonngren-wave equation: An integration of Painlevé analysis and Hirota bilinear method, *Rend. Fis. Acc. Lincei*, **36** (2025), 917–932. https://doi.org/10.1007/s12210-025-01354-0

AIMS Press

© 2026 the Author(s), licensee AIMS Press. This is an open access article distributed under the terms of the Creative Commons Attribution License (https://creativecommons.org/licenses/by/4.0)